### **OPEN ACCESS**



# Constraints on the X-Ray and Very-high-energy Gamma-Ray Flux from Supernova Remnant W44

```
A. Archer<sup>1</sup>, P. Bangale<sup>2</sup>, J. T. Bartkoske<sup>3</sup>, W. Benbow<sup>4</sup>, J. H. Buckley<sup>5</sup>, Y. Chen<sup>6</sup>, J. L. Christiansen<sup>7</sup>, A. J. Chromey<sup>4</sup>,
A. Archer¹, P. Bangale², J. T. Bartkoske³, W. Benbow³, J. H. Buckley³, Y. Chen³, J. L. Christiansen², A. J. Chromey³, A. Duerr³, M. Errando⁵, M. Escobar Godoy³, S. Feldman⁶, Q. Feng³, J. Foote², L. Fortson³, A. Furniss¹¹, W. Hanlon⁴, O. Hervet³, C. E. Hinrichs⁴, J. Holder², T. B. Humensky¹², J. W. Jin⁶, M. N. Johnson³, P. Kaaret¹⁴, J. M. Kertzman¹, M. Kherlakian¹⁶, D. Kieda³, T. K. Kleiner¹⁶, N. Korzoun², S. Kumar¹², S. Kumdu¹², M. J. Lang¹³, G. Maier¹⁶, M. Lundy¹, M. J. Millard¹⁴, C. L. Mooney², P. Moriarty¹, R. Mukherjee², W. Ning⁶, R. A. Ong⁶, M. Pohl¹6,²¹, E. Pueschel², J. Quinn², P. L. Rabinowitz⁵, K. Ragan¹, P. T. Reynolds², D. Ribeiro³, E. Roache⁴, L. Saha⁴, M. Santander¹, G. H. Sembroski², R. Shang², D. Tak², A. K. Talluri³, J. V. Tucci²,
                                                                  D. A. Williams<sup>8</sup>, S. L. Wong<sup>19</sup>, and J. Woo<sup>28</sup>
                          Department of Physics and Astronomy, DePauw University, Greencastle, IN 46135-0037, USA

Department of Physics and Astronomy and the Bartol Research Institute, University of Delaware, Newark, DE 19716, USA
                                                 Department of Physics and Astronomy, University of Utah, Salt Lake City, UT 84112, USA
                                                          Center for Astrophysics-Harvard & Smithsonian, Cambridge, MA 02138, USA
                                                             Department of Physics, Washington University, St. Louis, MO 63130, USA
                                             <sup>6</sup> Department of Physics and Astronomy, University of California, Los Angeles, CA 90095, USA
                                             Physics Department, California Polytechnic State University, San Luis Obispo, CA 94307, USA
                          <sup>8</sup> Santa Cruz Institute for Particle Physics and Department of Physics, University of California, Santa Cruz, CA 95064, USA

    School of Physics and Astronomy, University of Minnesota, Minneapolis, MN 55455, USA
    Department of Physics, California State University—East Bay, Hayward, CA 94542, USA

                                 <sup>11</sup> Department of Physics and Astronomy, Dartmouth College, 6127 Wilder Laboratory, Hanover, NH 03755, USA
                                                                Department of Physics, University of Maryland, College Park, MD, USA
                                                                     NASA Goddard Space Flight Center, Greenbelt, MD 20771, USA
                 Department of Physics and Astronomy, University of Iowa, Van Allen Hall, Iowa City, IA 52242, USA; matthew-j-millard@uiowa.edu

15 NASA Marshall Space Flight Center, Huntsville, AL 35812, USA

16 DESY, Platanenallee 6, 15738 Zeuthen, Germany
                                               <sup>17</sup> Department of Physics and Astronomy, University of Alabama, Tuscaloosa, AL 35487, USA
                                            18 School of Natural Sciences, University of Galway, University Road, Galway, H91 TK33, Ireland
                                                                Physics Department, McGill University, Montreal, QC H3A 2T8, Canada
                                            Department of Physics and Astronomy, Barnard College, Columbia University, NY 10027, USA
                                                <sup>21</sup> Institute of Physics and Astronomy, University of Potsdam, 14476 Potsdam-Golm, Germany Fakultät für Physik & Astronomie, Ruhr-Universität Bochum, D-44780 Bochum, Germany
                                                                School of Physics, University College Dublin, Belfield, Dublin 4, Ireland
                                    Department of Physical Sciences, Munster Technological University, Bishopstown, Cork, T12 P928, Ireland

25 Department of Physics and Astronomy, Purdue University, West Lafayette, IN 47907, USA
                                             <sup>26</sup> SNU Astronomy Research Center, Seoul National University, Seoul 08826, Republic of Korea
                                      <sup>27</sup> Department of Physics, Indiana University-Purdue University Indianapolis, Indianapolis, IN 46202, USA
                                                      Columbia Astrophysics Laboratory, Columbia University, New York, NY 10027, USA
                                          Received 2025 January 11; revised 2025 March 11; accepted 2025 March 11; published 2025 April 8
```

### **Abstract**

Observations of GeV gamma-ray emission from the well-studied mixed-morphology supernova remnant (SNR) W44 by Fermi-Large Area Telescope and AGILE imply that it is a site of significant cosmic-ray acceleration. The spectral energy distribution (SED) derived from the GeV data suggests that the gamma-ray emission likely originates from the decay of neutral pions generated by cosmic-ray interactions. It is essential to measure the SED of W44 in the X-ray and very-high-energy (VHE) gamma-ray bands to verify the hadronic origin of the emission and to gauge the potential contributions from leptonic emission. We report an upper limit of the nonthermal X-ray flux from W44 of 5  $\times$  10 $^{-13}$  erg cm $^{-2}$  s $^{-1}$  in the 0.5–8.0 keV band based on  $\sim$ 300 ks of XMM-Newton observations. The X-ray upper limit is consistent with previously estimated hadronic models, but in tension with the leptonic models. We estimate the VHE flux upper limit of  $\sim$ 1.2  $\times$  10 $^{-12}$  erg s $^{-1}$  cm $^{-2}$  in the 0.5–5.0 TeV range from W44 using data from the Very Energetic Radiation Imaging Telescope Array System. Our nondetection of W44 at VHE wavelengths is in agreement with observations from other imaging atmospheric Cherenkov telescopes and is perhaps consistent with the evolutionary stage of the SNR.

Unified Astronomy Thesaurus concepts: Gamma-ray astronomy (628); Supernova remnants (1667); High energy astrophysics (739)

### 1. Introduction

Supernovae (SNe) inject  $\sim 10^{51}$  erg into the interstellar medium (ISM) a few times per century in our Galaxy. If the remnants of SNe can convert  $\sim 10\%$  of the SN explosion energy to cosmic-ray energy, it would suffice to explain the

locally observed cosmic-ray population up to the cosmic-ray spectrum knee at 3 PeV (C. D. Dermer & G. Powale 2013). This energy conversion may be achieved in the expanding shockwaves of supernova remnants (SNRs) through diffusive shock acceleration, where charged particles gain energy by repeatedly crossing the SNR shock front via scattering off regions of magnetic turbulence (E. Fermi 1949; A. R. Bell 1978; S. P. Reynolds 2008). One of the difficulties in observationally confirming that SNRs are cosmic-ray accelerators is verifying that gamma-ray emission is of hadronic (not leptonic) origin. SNR W44 (G34.7-0.4) has one of the strongest lines of evidence that the observed gamma-ray emission results from hadronic cosmic-ray interactions.

W44 is a prototypical mixed-morphology SNR (J. Rho & R. Petre 1998), featuring a well-defined elliptical radio shell (J. P. Hollinger & R. W. Hobbs 1966; E. B. Giacani et al. 1997; G. Castelletti et al. 2007), and strong thermal X-ray emission toward the center (I. M. Harrus et al. 1997; J. Rho & R. Petre 1998; R. L. Shelton et al. 2004; H. Uchida et al. 2012; H. Okon et al. 2020). Timing measurements of the radio pulsar PSR B1853+01 associated with the remnant suggest a spin-down age of  $\sim 20,000 \,\mathrm{yr}$  (A. Wolszczan et al. 1991; I. M. Harrus et al. 1997). W44 has been firmly detected with the high-energy gamma-ray telescopes AGILE (A. Giuliani et al. 2011) and the Fermi Large Area Telescope (LAT; A. A. Abdo et al. 2010). The best-fit gamma-ray morphology from Fermi-LAT is an elliptical ring with a semimajor axis of 0.3 that matches well with the radio shell (A. A. Abdo et al. 2010; G. Peron et al. 2020). The spectrum of W44 rises steeply up to ~200 MeV, known as the "pion bump" (M. Ackermann et al. 2013; G. Peron et al. 2020), indicating that the emission originates from the decay of neutral pions produced from energetic proton-proton collisions.

Analyses of CO line emission in the vicinity of W44 suggest that the SNR blastwave interacts with dense molecular clouds (M. Seta et al. 1998, 2004; S. Paron et al. 2009; T. Sashida et al. 2013; S. Yoshiike et al. 2013). Two regions of distinct GeV gamma-ray emission were detected to the southeast and northwest of the SNR (Y. Uchiyama et al. 2012; G. Peron et al. 2020). The origin of the emission is unclear, but it may be the result of energetic cosmic rays that escape the shock from W44 and interact with nearby gas clouds or dense ISM.

W44 is one of the brightest SNRs detected with Fermi-LAT, yet a detection at TeV energies remains elusive. Nonthermal X-ray emission, which may help constrain hadronic emission models, has also not been detected from W44. Here, we present the results of our study of W44 using observations from the Very Energetic Radiation Imaging Telescope Array System (VERITAS) and XMM-Newton. In Section 2, we present the details of the observations and data processing. In Section 3, we describe our analyses of the X-ray and very-high-energy (VHE; >100 GeV) spectra and results. In Section 4, we discuss the results and their implications for the multi-wavelength spectral energy distribution (SED). Section 5 summarizes our findings from our VHE and X-ray analyses of W44.

### 2. Observations

# 2.1. VERITAS

VERITAS is an array of four imaging atmospheric Cherenkov telescopes located at the base of Mt. Hopkins in Amado, AZ, USA (31°40′N, 110°57′W). Each of the four

telescopes in the VERITAS array has a 12 m diameter optical reflector, consisting of 350 hexagonal spherical mirror segments. The telescopes are spaced, depending on the observing epoch, between 35 and 170 m apart, allowing for stereoscopic observation of the Cherenkov light produced from the shower of secondary particles created from VHE gamma rays interacting with the atmosphere. The mirror placements follow the Davies-Cotton design (J. M. Davies & E. S. Cotton 1957), for a total reflecting area of 110 m<sup>2</sup>. The mirrors focus the Cherenkov light produced from gamma-ray showers onto a camera box at the focal point of the reflector, 12 m from the center of the dish. The camera consists of 499 Hamamatsu R10560-100-20 26 mm diameter photomultipler tubes, which give a field of view of 3.5. The spatial resolution of VERITAS is 0.08 on the sky at 1 TeV. The array is capable of detecting a point source with 1% of the Crab flux after observing it for 25 hr. VERITAS is currently sensitive to photons with energies ranging from 85 GeV to 30 TeV.

We observed W44 with VERITAS in wobble mode for 10 hr and 3.6 hr in May–June of 2008 and 2016, respectively. For each observing run (38 in total), we pointed the array to a position offset 0°.5, alternating north, south, east, and west from the target position of  $\alpha_{2000}=284^\circ.141,~\delta_{2000}=1^\circ.31078$  in 2008 and  $\alpha_{2000}=284^\circ.141,~\delta_{2000}=1^\circ.32182$  in 2016 to characterize the detector background rate. We excluded the north wobble data because source-free background measurements were not possible. We applied the standard VERITAS event reconstruction to the remaining data and inspected each run for rate, timing, and tracking consistency. Runs that pass our initial assessment are subjected to further analysis, while rejected runs are not considered. The resulting effective exposure time is 9.6 hr.

#### 2.2. XMM-Newton

XMM-Newton observed W44 in 2013 for a total of 335.5 ks. We use data from the three Obs. IDs of this observation: 0721630101, 0721630201, and 0721630301. We focus on the data obtained from the European Photon Imaging Camera (EPIC), which includes two Metal Oxide Semiconductor (MOS) cameras (M. J. L. Turner et al. 2001) and a pn CCD camera (L. Strüder et al. 2001). Due to the poor coverage of the MOS1 camera due to meteoroid strikes disabling two of the chips (CCD3 and CCD6) and the higher background count rate of the pn camera, we use data only from the MOS2 camera. We processed the data with the Science Analysis System (SAS) software version 20.0 and the calibration database version 3.13, following the guidelines for extended sources analysis (ESAS) procedures. <sup>29</sup> A total exposure time of 297 ks remained after we performed data quality checks. We generated redistribution matrix files and ancillary response files using the mos-spectra command and estimated the non-X-ray background (NXB) using mos-back.

# 3. Analysis and Results

### 3.1. VERITAS

We processed the data using standard VERITAS analysis techniques, including a Hillas parameter analysis (A. M. Hillas 1985). We applied analysis cuts to the mean scaled length, mean scaled width, and integrated charge in the signal to help distinguish between events of cosmic-ray and gamma-ray

https://heasarc.gsfc.nasa.gov/docs/xmm/esas/cookbook/xmm-esas.html

origins. We performed the event reconstruction with the Eventdisplay software (G. Maier & J. Holder 2017) and converted the data to DL3 fits files compatible with the Gammapy (v1.1; A. Aguasca-Cabot et al. 2023; A. Donath et al. 2023) software for further analysis. Our spectral energy threshold is 0.4 TeV. We extracted the spectrum from a circle of radius  $\theta = 0.3$ , centered on the approximate radioimage position of W44 ( $\alpha_{2000} = 284.015$ ,  $\delta_{2000} = 1.349$ ). For the background spectrum, we selected between two and three locations within the field of view according to the reflected regions method (see D. Berge et al. 2007). This method does not rely on accounting for the radial dependence of the background acceptance. The statistical significance of any excess is evaluated using the likelihood method described by T. P. Li & Y. O. Ma (1983), which takes into account the counts from the on-source and background regions and their different acceptances.

We find no significant source emission at the location of W44. We estimate a differential flux upper limit of  $\sim\!1.2\times10^{-12}\,\mathrm{erg\,s^{-1}\,cm^{-2}}$  in the 0.5–5.0 TeV range, for a power-law model with a spectral index of 2.4. The upper limit in each energy bin corresponds to a 95% confidence level using the Wstat $^{30}$  test-statistic value. Our flux upper limits agree well with a power-law extrapolation of the Fermi-LAT data from G. Peron et al. (2020) and are somewhat more constraining than the H.E.S.S. upper limit in the 1–10 TeV band (H. E. S. S. Collaboration et al. 2018).

#### 3.2. XMM-Newton

We extracted the XMM MOS2 spectrum from a region coinciding with the observed GeV gamma-ray ring-like emission from W44 (see the magenta region in Figure 1). We fitted the 0.5-8 keV spectrum with an absorbed X-ray emission spectral model assuming two variable recombining nonequilibrium ionization plasma models, tbabs \* (vrnei + vrnei), using the XSPEC software package (K. A. Arnaud 1996). We also included a Gaussian line at ~1.25 keV to account for unknown excess emission possibly due to missing Fe L lines in the atomic data (N. S. Brickhouse et al. 2000). Figure 2 shows the extracted spectrum and our best-fit emission + background model. We subtracted the NXB from the spectrum and estimated the X-ray background emission by modeling the spectrum extracted from the white region in Figure 1. Our background model includes the following components: foreground emission, Galactic ridge X-ray emission, the cosmic X-ray background, and Al and Si K $\alpha$  instrumental lines.

Our best-fit vrnei model parameters are summarized in Table 1. In our lower-kT vrnei model, the Ne, Mg, Si, S, and Fe abundances are allowed to vary. The Ni abundance is tied to the Fe abundance, while the Ar and Ca abundances are tied to the S abundance. In the higher-kT vrnei model, the abundances are fixed at solar values (J. Wilms et al. 2000). The two absorbed vrnei components can reasonably account for the observed source emission in the X-ray spectrum of W44 with  $\chi^2/{\rm degrees}$  of freedom = 684/716.

To estimate an upper limit on the nonthermal emission from W44, we added a power-law component to our model. We fixed the photon index at the standard value for SNRs,  $\Gamma=2$ . Using the steppar command in XSPEC, we increased the

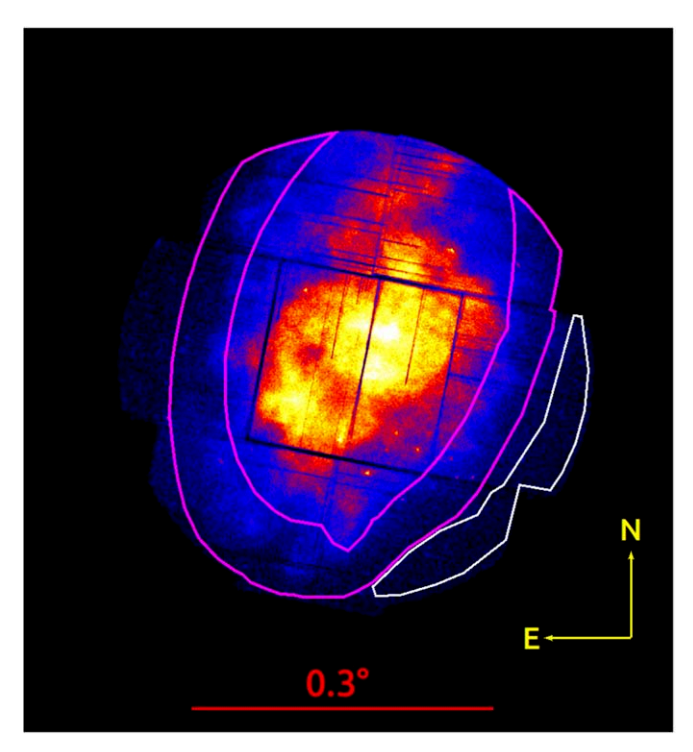


**Figure 1.** XMM MOS2 counts image of supernova remnant W44 in the 0.5–8 keV band smoothed with a Gaussian kernel of radius =  $3^{''}$ .3 and  $\sigma = 1^{''}$ .7 We extracted the target spectrum from the magenta region and the background spectrum from the white region.

power-law flux until the  $\chi^2$  statistic reached the value corresponding to the 99% confidence level above the minimum, giving a flux value of  $2.8 \times 10^{-13}\,\mathrm{erg\,cm^{-2}\,s^{-1}}$ . Although the shape of our extraction region is based on the best-fit ring found by G. Peron et al. (2020), it only covers about 60% of the ring area due to the constraint of the XMM MOS field of view. To account for the lack of coverage, we multiply our estimated upper limit by a factor of 1.7. Thus, we estimate a flux upper limit  $\sim$ 5  $\times$   $10^{-13}\,\mathrm{erg\,cm^{-2}\,s^{-1}}$  in the 0.5–8.0 keV band.

To test the effect of the photon index on the upper limit, we tried several values, from  $\Gamma=1.2$  to 2.8. For  $\Gamma\gtrsim 2.4$  and  $\Gamma\lesssim 1.6$ , the resulting change in upper limit is enough to affect our conclusions regarding the preferred multiwavelength emission model (discussed in Section 4). However, we note that the measured photon indices of other mixed-morphology SNRs with potential nonthermal emission, W28 and G346.6-0.2, are  $\Gamma\sim 2$  (P. Zhou et al. 2014; K. Auchettl et al. 2017). Moreover, higher photon indices ( $\Gamma\gtrsim 2.5$ ) are generally expected only for younger SNRs, less than a few thousand years old. Thus, our choice of  $\Gamma=2$  is suitable for W44, a  $\sim\!\!2\times10^4\,\mathrm{yr}$  old mixed-morphology SNR.

# 4. Discussion

## 4.1. Multiwavelength SED

A. Giuliani et al. (2011) modeled the SED of W44 using radio (G. Castelletti et al. 2007), AGILE, and Fermi-LAT data. The authors tested both hadronic- and leptonic-based models and found that a hadronic model fit best for cosmic rays interacting with a gas of density  $n_o = 100 \, \mathrm{cm}^{-3}$ . M. Cardillo et al. (2014) analyzed a newer AGILE data set together with CO data from the NANTEN2 telescope and found a similar result. The best-fit hadronic (a broken power law with  $p_1 = 2.2$ ,

<sup>30</sup> https://docs.gammapy.org/dev/api/gammapy.stats.wstat.html#gammapy.stats.wstat

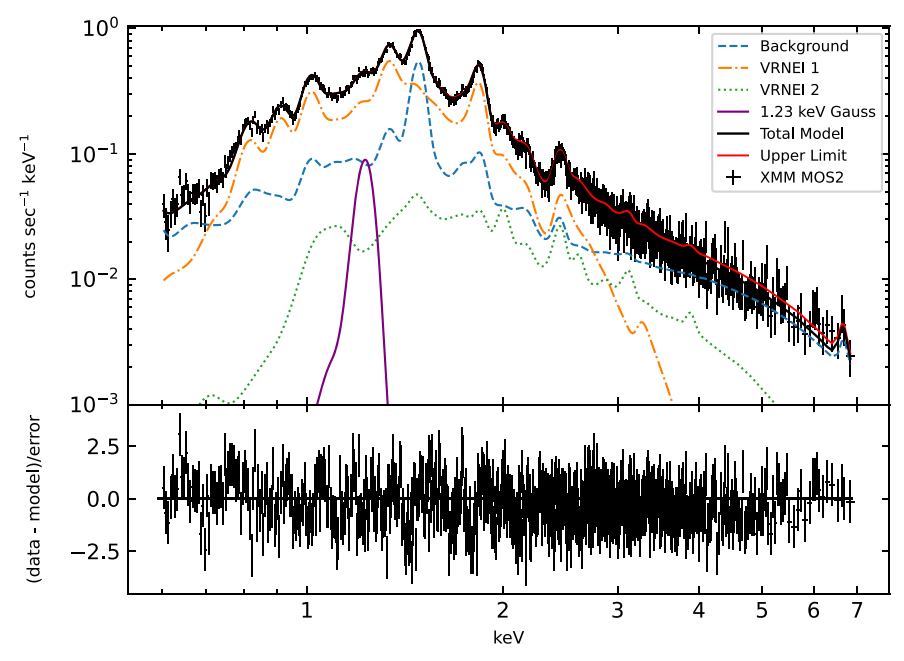


Figure 2. XMM-Newton MOS2 spectrum extracted from the radio boundary of SNR W44 (magenta region in Figure 1) with our best-fit model overlaid (solid black curve). The solid red curve shows the best-fit model with the nonthermal flux upper limit included.

 Table 1

 Best-fit X-Ray Spectral Model Parameters

Component	Parameter	Value
$N_{\rm H}~({\rm cm}^{-2})$		$2.32 \pm 0.10 \times 10^{21}$
vrnei	$kT_e$ (keV)	$0.215^{+0.004}_{-0.007}$
	$n_e t \text{ (cm}^{-3} \text{ s)}$	$8.28^{+0.81}_{-0.76} \times 10^{11}$
	Norm	$0.12 \pm 0.04$
	Ne	$4.1^{+3.0}_{-1.5}$
	Mg	$2.8^{+1.7}_{-0.9}$
	Si	$5.6^{+13.9}_{-1.9}$
	S	$5.8_{-2.6}^{+4.8}$
	Fe	$4.6^{+4.9}_{-2.1}$
vrnei	$kT_e$ (keV)	$1.70_{-0.34}^{+0.66}$
	$n_e t \text{ (cm}^{-3} \text{ s)}$	$2.12^{+6.74}_{-1.34} \times 10^{11}$
	Norm	$0.003 \pm 0.001$

Note. Elemental abundances are relative to solar values (J. Wilms et al. 2000).

 $p_2=3.2$ , and  $E_{\rm break}=20~{\rm GeV}$ ) and leptonic (smoothed broken power laws, with  $p_1'=-2.5,\,p_2'=3.4$ , and  $E_{\rm break}=0.5~{\rm GeV}$ ) SED models from M. Cardillo et al. (2014) are shown in Figure 3. The leptonic models are dominated by bremsstrahlung emission at gamma-ray wavelengths. The hadronic model also includes a weak bremsstrahlung component. G. Peron et al. (2020) similarly found that a hadronic model was the best fit for the gamma-ray SED based on 9.7 yr of Fermi-LAT data. Thus, model fitting of the SED of W44 strongly suggests that the emission is hadronic in origin, likely from cosmic rays accelerated by the SNR blast wave encountering dense gas clouds, interacting via proton-proton reactions, and producing neutral pions that decay via gamma-ray emission. Confirmation of the hadronic emission scenario with the multiwavelength SED is essential, since a pion bump feature can also originate from diffuse gamma-ray emission of the Galactic plane (S. D. Hunter et al. 1997). Our nonthermal X-ray flux upper limit is plotted along with the best-fit hadronic model from

M. Cardillo et al. (2014) in Figure 3. Our upper limit slightly favors the best-fit hadronic models over the leptonic models from M. Cardillo et al. (2014).

Initial gamma-ray observations of W44 with the Energetic Gamma-Ray Experiment Telescope (EGRET) on board the Compton Gamma-Ray Observatory found flux levels potentially consistent with cosmic-ray acceleration up to PeV energies (J. A. Esposito et al. 1996). The model flux from J. H. Buckley et al. (1998), estimated from EGRET measurements and extrapolated to PeV energies, is shown by the gray dotted curve in Figure 3. However, flux upper limits estimated from follow-up observations with the Whipple telescope were well below the expected TeV flux level (J. H. Buckley et al. 1998). Although W44 is one of the brightest SNRs observed at GeV energies (F. Acero et al. 2016), the flux decreases with a power-law index of  $3.3 \pm 0.4$  above  $10 \, \text{GeV}$  (G. Peron et al. 2020), suggesting that W44 should be relatively faint at VHE wavelengths.

Our VERITAS flux upper limit does not constrain the predicted emission models of M. Cardillo et al. (2014) and G. Peron et al. (2020), which fall off steeply above 10 GeV. Observations of the W44 region with significantly deeper exposures using the High Energy Stereoscopic System (H.E.S.S.) and the Major Atmospheric Gamma Imaging Cherenkov telescopes have also not yielded a detection of W44 (H. E. S. S. Collaboration et al. 2018; R. di Tria et al. 2022) at VHE wavelengths. R. Brose et al. (2020) modeled the evolution of the cosmic-ray spectrum inside a SNR up to an age of 105 yr. The leptonic emission declines more rapidly than the hadronic emission due to energy losses of electrons. However, after 10<sup>4</sup> yr, the hadronic flux would also be low, and thus older remnants can be seen only when the gas density is high. Hence, the interaction of old SNRs with massive molecular clouds may be needed to produce significant VHE gamma-ray emission. R. Brose et al. (2021) produced simulated gamma-ray SEDs for test SNRs assuming a distance of 1 kpc. After 10<sup>4</sup> yr, the SED appears soft, owing to a rapid decline in the maximum energy to which the shock can currently accelerate particles. Considering the estimated age of W44 of  $\sim$ 20 kyr, this could be the case in W44 as well.

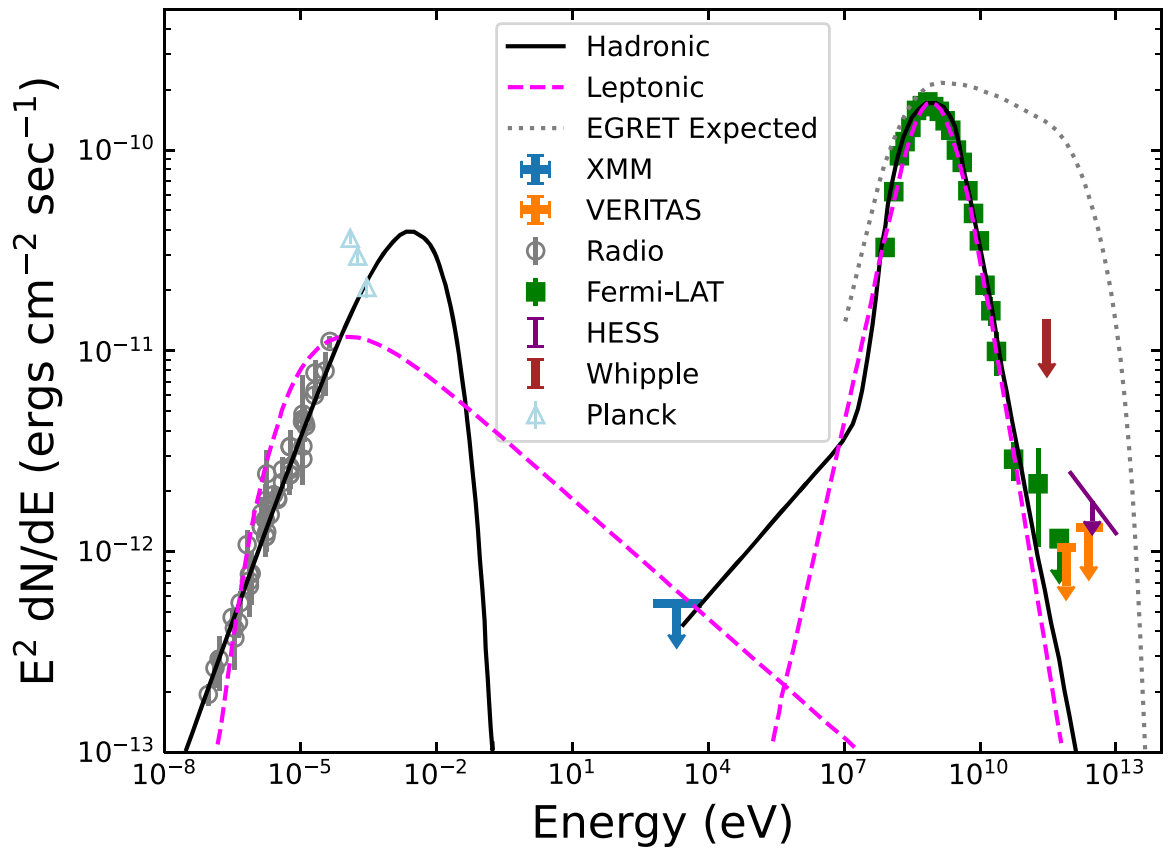


**Figure 3.** Multiwavelength SED of W44. Radio data are from G. Castelletti et al. (2007), Planck data from Planck Collaboration et al. (2016), Fermi-LAT data from G. Peron et al. (2020), and H.E.S.S. upper limits from H. E. S. S. Collaboration et al. (2018). The overlaid best-fit hadronic (solid black lines) and leptonic model (dashed magenta lines) are adapted from Figures 4 and 5 of M. Cardillo et al. (2014) and correspond to models "H3" and "L2," respectively, in their Table 3. The hadronic model includes a bremsstrahlung component, which dominates from ~10<sup>3</sup> to 10<sup>7</sup> eV The gray dotted line denotes the expected emission model from EGRET observations, adapted from Figure 8 of J. H. Buckley et al. (1998). The XMM-Newton and VERITAS upper limits are from this work.

IC 443 is another SNR that shows evidence of significant spectral curvature in the GeV band and a hadronic origin for the gamma-ray emission (M. Tavani et al. 2010). Interestingly, W44 and IC 443 are both mixed-morphology SNRs on the order of 10<sup>4</sup> yr old. However, IC 443 has been firmly detected in the VHE range (J. Albert et al. 2007; V. A. Acciari et al. 2009). The difference in VHE flux levels is perhaps due to the age of the SNRs. The age estimates for IC 443 vary significantly, from 3 kyr (R. Petre et al. 1988) to 30 kyr (R. A. Chevalier 1999; C. M. Olbert et al. 2001). Thus, IC 443 may be in a younger evolutionary stage than W44.

# 4.2. Thermal X-Ray Emission at the SNR Boundary

The hadronic models for gamma-ray emission strongly depend on the assumed ambient density around the cosmic-ray source. Both high- and low-density scenarios have been considered by M. Cardillo et al. (2014) and G. Peron et al. (2020), respectively, when modeling the hadronic gamma-ray flux. Both studies use a broken power-law function to model the proton spectrum. However, M. Cardillo et al. (2014) found a best-fit ambient density of  $300\,\mathrm{cm}^{-3}$  for a distance,  $d=3.1\,\mathrm{kpc}$  (D. H. Clark & J. L. Caswell 1976; A. Wolszczan et al. 1991), while G. Peron et al. (2020) found  $n_o=10\,\mathrm{cm}^{-3}$  for  $d=2.2\,\mathrm{kpc}$ . Although their best-fit ambient densities and assumed distances are different, M. Cardillo et al. (2014) and G. Peron et al. (2020) report a similar total proton energy in the remnant,  $W_p$ , with values of  $5\times10^{49}\,\mathrm{erg}$  and  $1.2\times10^{49}\,\mathrm{erg}$ 

respectively, with both models fitting the gamma-ray SED reasonably well. This is possible because  $W_p$  is proportional to the square of the distance and inversely proportional to density.

We can use our model of the thermal X-ray emission at the boundary of W44 to estimate the ambient density around the expanding SNR by applying the equation for ram pressure,  $P_{\rm ram} \approx \rho_o(V_s)^2$ , where  $V_s$  is the shock speed, and  $\rho_o$  is the ambient mass density. The ion pressure interior to the shock boundary should be equal to the ram pressure,  $P_{\rm ram} = P_{\rm ion} \approx n_{\rm ion}(kT_{\rm ion})$ , where  $n_{\rm ion}$  and  $kT_{\rm ion}$  are the ion number density and temperature, respectively. Thus, we can solve for the ambient number density,  $n_o = \rho_o/m_{\rm H} = n_{\rm ion}(kT_{\rm ion})/(m_{\rm H}V_s^2)$ , where  $m_{\rm H}$  is the mass of hydrogen.

The lower-kT vrnei component dominates our model, with temperature  $kT_e \sim 0.2$  keV and ionization timescale  $n_e t \sim 8 \times 10^{11}$  s cm<sup>-3</sup>. The high ionization timescale (nearly  $10^{12}$  s cm<sup>-3</sup>) suggests that W44 is approaching collisional ionization equilibrium. Thus, the electrons and ions would have similar temperatures, kT<sub>e</sub>  $\approx kT_{\rm ion} = 0.2$  keV. The electron density,  $n_e$ , may be determined if the time since the plasma was shocked, t, is known. Using a conservative t of  $10^4$  yr gives an electron number density,  $n_e \sim 2$  cm<sup>-3</sup>. However, based on CO line emission, S. Anderl et al. (2014) estimated the age of shocks in the northeast of the remnant to be as young as  $\sim 10^3$  yr, which would imply  $n_e \sim 20$  cm<sup>-3</sup>. Assuming solar elemental abundances for the emitting plasma,  $n_e = 1.2n_{\rm H}$ , where  $n_{\rm H}$  is the number density of hydrogen in the plasma. Solving for  $n_{\rm H}$ ,

and given that  $n_{\rm H} \approx n_{\rm ion}$ , then  $n_{\rm ion} = 1.67 - 16.7 \, {\rm cm}^{-3}$ , which implies  $P_{\rm ram} = 5.4 \times 10^{-10} - 54 \times 10^{-10} \, {\rm dyn \, cm}^{-2}$ .

B.-C. Koo & C. Heiles (1995) found that the shell of H I gas around W44 has an expansion speed,  $V_s = 150 \text{ km s}^{-1}$ . This is generally taken to be the forward shock speed for W44 (D. P. Cox et al. 1999; X. Tang & R. A. Chevalier 2015). However, inserting this value into our equation for ram pressure gives a postshock to preshock density (compression) ratio of approximately unity, instead of the factor of 4 expected for a strong shock in adiabatic conditions. We note that B.-C. Koo & C. Heiles (1995) suggested that the H I shell was separate from the radio continuum shell, for which they estimated an expansion speed of 330 km s $^{-1}$ . R. L. Shelton et al. (1999) also estimated shock speeds up to  $\sim$ 300 km s $^{-1}$  for the tenuous region of W44. Thus, we assume  $V_s = 300 \text{ km s}^{-1}$ , which gives a compression ratio,  $n_{\text{ion}}/n_o = 4.6$ , much closer to the expected ratio. We estimate the ambient density to be between 0.36 and  $3.6 \text{ cm}^{-3}$ . Our value is in agreement with D. P. Cox et al. (1999), who found an ambient density of about 6 cm<sup>-3</sup> using ROSAT data, assuming that the shell formation time equals the age. Thus, the density estimated from our X-ray measurements is more consistent with the scenario of a closer distance of  $\sim 2 \,\mathrm{kpc}$ to W44.

We note that CO line measurements of molecular gas around W44 (S. Yoshiike et al. 2013) suggest that the molecular proton density is about 200 cm<sup>-3</sup> on average. The submillimeter density estimate includes some high-density knots, which could dominate the average, causing it to be significantly higher than the X-ray estimate. For such a high average density, the Sedov radius and postshock temperature would be too small compared to what we observe. In this scenario, the shock likely initially passed through low-density material in a wind-blown bubble created by the SN progenitor, where the shock was fast (S. Das et al. 2024). The forward shock would eventually interact with the dense gas, slow down until  $T_e$  is too small for X-ray emission, and effectively produce gamma-rays in the highdensity environment. S. Das et al. (2024) found that the spectral index for pion-decay emission would exhibit a soft proton spectra, reaching 2.4-2.6 above 10 GeV, similar to the soft gamma-ray spectrum observed in W44.

## 5. Conclusions

We investigated the X-ray and VHE emission from SNR W44 using data from the XMM-Newton and VERITAS telescopes to better understand the origin of the multiwavelength emission. Our analysis of the X-ray spectrum at the boundary of the SNR did not reveal the presence of nonthermal emission coincident with observed GeV emission. However, we note that our nonthermal X-ray flux upper estimate of 5  $\times$  10<sup>-13</sup> erg cm<sup>-2</sup> s<sup>-1</sup> is consistent with the hadronic model and is in tension with the leptonic model from M. Cardillo et al. (2014). We used our best-fit model of the thermal X-ray-emitting plasma to estimate the ambient density around the SNR. Our density estimate is generally consistent with other X-ray analyses and may favor a distance of  $\sim$ 2 kpc to W44 when modeling the gamma-ray SED assuming a hadronic origin. Based on its bright GeV emission, it was perhaps expected that W44 might be a contributor of Galactic PeV cosmic rays. However, our analysis of the VERITAS observations of W44 also did not result in a detection. Our flux upper limit slightly improves upon the Fermi-LAT and H.E.S.S. upper limits in the TeV band, and confirms that W44

is significantly fainter in the TeV compared to the GeV band. Future gamma-ray observatories, like the Cherenkov Telescope Array Observatory (CTAO), may be able to detect W44 in the VHE regime. The expected flux sensitivity of the CTAO, based on a 50 hr exposure, is similar to the expected flux from W44 from 0.1 to 1.0 TeV (Cherenkov Telescope Array Consortium et al. 2019). Thus, an exposure of this duration could constrain the current best-fit emission models. W44 is an exemplary case of a Sedov phase SNR emitting in gamma-rays via hadronic interactions. The presence of a cutoff below TeV energies points to questions about the acceleration mechanism and propagation models that suggest SNRs are able to produce cosmic rays with energies up to the knee of the locally observed cosmic-ray spectrum.

### Acknowledgments

This research is supported by grants from the U.S. Department of Energy Office of Science, the U.S. National Science Foundation and the Smithsonian Institution, by NSERC in Canada, and by the Helmholtz Association in Germany. This research used resources provided by the Open Science Grid, which is supported by the National Science Foundation (NSF) and the U.S. Department of Energy's Office of Science, and resources of the National Energy Research Scientific Computing Center (NERSC), a U.S. Department of Energy Office of Science User Facility operated under Contract No. DE-AC02-05CH11231. We acknowledge the excellent work of the technical support staff at the Fred Lawrence Whipple Observatory and at the collaborating institutions in the construction and operation of the instrument. M. M. thanks NSF for support under grant PHY-2012916. We are grateful for the suggestions provided by the anonymous referee, which helped us to improve the clarity and quality of this work.

Facilities: VERITAS, XMM.

Software: astropy (Astropy Collaboration et al. 2013, 2018), Eventdisplay (G. Maier & J. Holder 2017), Gammapy (A. Donath et al. 2023), XSPEC (K. A. Arnaud 1996).

# ORCID iDs

P. Bangale https://orcid.org/0000-0002-3886-3739 J. T. Bartkoske https://orcid.org/0000-0002-9675-7328 W. Benbow https://orcid.org/0000-0003-2098-170X J. H. Buckley https://orcid.org/0000-0001-6391-9661 Y. Chen https://orcid.org/0009-0001-5719-936X A. Duerr https://orcid.org/0000-0003-1716-4119 M. Errando https://orcid.org/0000-0002-1853-863X Q. Feng https://orcid.org/0000-0001-6674-4238 J. Foote https://orcid.org/0000-0002-2944-6060 L. Fortson https://orcid.org/0000-0002-1067-8558 A. Furniss https://orcid.org/0000-0003-1614-1273 W. Hanlon https://orcid.org/0000-0002-0109-4737 O. Hervet https://orcid.org/0000-0003-3878-1677 C. E. Hinrichs https://orcid.org/0000-0001-6951-2299 J. Holder https://orcid.org/0000-0002-6833-0474 T. B. Humensky https://orcid.org/0000-0002-1432-7771 W. Jin https://orcid.org/0000-0002-1089-1754 M. N. Johnson https://orcid.org/0009-0008-2688-0815 P. Kaaret https://orcid.org/0000-0002-3638-0637 D. Kieda https://orcid.org/0000-0003-4785-0101 T. K. Kleiner https://orcid.org/0000-0002-4260-9186 N. Korzoun https://orcid.org/0000-0002-4289-7106 S. Kumar https://orcid.org/0000-0002-5167-1221

M. J. Lang https://orcid.org/0000-0003-4641-4201 G. Maier https://orcid.org/0000-0001-9868-4700 M. Lundy https://orcid.org/0000-0003-3802-1619 M. J. Millard https://orcid.org/0000-0001-7106-8502 C. L. Mooney https://orcid.org/0000-0001-5937-446X P. Moriarty https://orcid.org/0000-0002-1499-2667 R. Mukherjee https://orcid.org/0000-0002-3223-0754 W. Ning https://orcid.org/0000-0002-6121-3443 R. A. Ong https://orcid.org/0000-0002-4837-5253 M. Pohl https://orcid.org/0000-0001-7861-1707 E. Pueschel https://orcid.org/0000-0002-0529-1973 J. Quinn https://orcid.org/0000-0002-4855-2694 K. Ragan https://orcid.org/0000-0002-5351-3323 D. Ribeiro https://orcid.org/0000-0002-7523-7366 L. Saha https://orcid.org/0000-0002-3171-5039 R. Shang https://orcid.org/0000-0002-9856-989X D. Tak https://orcid.org/0000-0002-9852-2469 D. A. Williams https://orcid.org/0000-0003-2740-9714 S. L. Wong https://orcid.org/0000-0002-2730-2733 J. Woo https://orcid.org/0009-0001-6471-1405

#### References

```
Abdo, A. A., Ackermann, M., Ajello, M., et al. 2010, Sci, 327, 1103
Acciari, V. A., Aliu, E., Arlen, T., et al. 2009, ApJL, 698, L133
Acero, F., Ackermann, M., Ajello, M., et al. 2016, ApJS, 224, 8
Ackermann, M., Ajello, M., Allafort, A., et al. 2013, Sci, 339, 807
Aguasca-Cabot, A., Donath, A., Feijen, K., et al. 2023, Gammapy: Python Toolbox
   for Gamma-ray Astronomy, v1.1, Zenodo, doi:10.5281/zenodo.8033275
Albert, J., Aliu, E., Anderhub, H., et al. 2007, ApJL, 664, L87
Anderl, S., Gusdorf, A., & Güsten, R. 2014, A&A, 569, A81
Arnaud, K. A. 1996, in ASP Conf. Ser. 101, Astronomical Data Analysis
   Software and Systems V, ed. G. H. Jacoby & J. Barnes (San Francisco, CA:
   ASP), 17
Astropy Collaboration, Price-Whelan, A. M., Sipőcz, B. M., et al. 2018, AJ,
   156, 123
Astropy Collaboration, Robitaille, T. P., Tollerud, E. J., et al. 2013, A&A,
   558, A33
Auchettl, K., Ng, C. Y., Wong, B. T. T., Lopez, L., & Slane, P. 2017, ApJ,
  847, 121
Bell, A. R. 1978, MNRAS, 182, 147
Berge, D., Funk, S., & Hinton, J. 2007, A&A, 466, 1219
Brickhouse, N. S., Dupree, A. K., Edgar, R. J., et al. 2000, ApJ, 530, 387
Brose, R., Pohl, M., & Sushch, I. 2021, A&A, 654, A139
Brose, R., Pohl, M., Sushch, I., Petruk, O., & Kuzyo, T. 2020, A&A, 634, A59
Buckley, J. H., Akerlof, C. W., Carter-Lewis, D. A., et al. 1998, A&A,
  329, 639
Cardillo, M., Tavani, M., Giuliani, A., et al. 2014, A&A, 565, A74
```

```
Castelletti, G., Dubner, G., Brogan, C., & Kassim, N. E. 2007, A&A, 471, 537
Cherenkov Telescope Array Consortium, Acharya, B. S., Agudo, I., et al. 2019,
  Science with the Cherenkov Telescope Array (Singapore: World Scientific)
Chevalier, R. A. 1999, ApJ, 511, 798
Clark, D. H., & Caswell, J. L. 1976, MNRAS, 174, 267
Cox, D. P., Shelton, R. L., Maciejewski, W., et al. 1999, ApJ, 524, 179
Das, S., Brose, R., Pohl, M., Meyer, D. M. A., & Sushch, I. 2024, A&A,
Davies, J. M., & Cotton, E. S. 1957, SoEn, 1, 16
Dermer, C. D., & Powale, G. 2013, A&A, 553, A34
di Tria, R., di Venere, L., Giordano, F., et al. 2022, ICRC (Berlin), 37, 642
Donath, A., Terrier, R., Remy, Q., et al. 2023, A&A, 678, A157
Esposito, J. A., Hunter, S. D., Kanbach, G., & Sreekumar, P. 1996, ApJ,
  461, 820
Fermi, E. 1949, PhRv, 75, 1169
Giacani, E. B., Dubner, G. M., Kassim, N. E., et al. 1997, AJ, 113, 1379
Giuliani, A., Cardillo, M., Tavani, M., et al. 2011, ApJL, 742, L30
H. E. S. S. Collaboration, Abdalla, H., Abramowski, A., et al. 2018, A&A,
  612, A3
Harrus, I. M., Hughes, J. P., Singh, K. P., Koyama, K., & Asaoka, I. 1997, ApJ,
Hillas, A. M. 1985, ICRC (La Jolla), 3, 445
Hollinger, J. P., & Hobbs, R. W. 1966, Sci, 153, 1633
Hunter, S. D., Bertsch, D. L., Catelli, J. R., et al. 1997, ApJ, 481, 205
Koo, B.-C., & Heiles, C. 1995, ApJ, 442, 679
Li, T. P., & Ma, Y. Q. 1983, ApJ, 272, 317
Maier, G., & Holder, J. 2017, ICRC (Busan), 35, 747
Okon, H., Tanaka, T., Uchida, H., et al. 2020, ApJ, 890, 62
Olbert, C. M., Clearfield, C. R., Williams, N. E., Keohane, J. W., & Frail, D. A.
  2001, ApJL, 554, L205
Paron, S., Ortega, M. E., Rubio, M., & Dubner, G. 2009, A&A, 498, 445
Peron, G., Aharonian, F., Casanova, S., Zanin, R., & Romoli, C. 2020, ApJL,
   896, L23
Petre, R., Szymkowiak, A. E., Seward, F. D., & Willingale, R. 1988, ApJ,
  335, 215
Planck Collaboration, Arnaud, M., Ashdown, M., et al. 2016, A&A, 586, A134
Reynolds, S. P. 2008, ARA&A, 46, 89
Rho, J., & Petre, R. 1998, ApJL, 503, L167
Sashida, T., Oka, T., Tanaka, K., et al. 2013, ApJ, 774, 10
Seta, M., Hasegawa, T., Dame, T. M., et al. 1998, ApJ, 505, 286
Seta, M., Hasegawa, T., Sakamoto, S., et al. 2004, AJ, 127, 1098
Shelton, R. L., Cox, D. P., Maciejewski, W., et al. 1999, ApJ, 524, 192
Shelton, R. L., Kuntz, K. D., & Petre, R. 2004, ApJ, 611, 906
Strüder, L., Briel, U., Dennerl, K., et al. 2001, A&A, 365, L18
Tang, X., & Chevalier, R. A. 2015, ApJ, 800, 103
Tavani, M., Giuliani, A., Chen, A. W., et al. 2010, ApJL, 710, L151
Turner, M. J. L., Abbey, A., Arnaud, M., et al. 2001, A&A, 365, L27
Uchida, H., Koyama, K., Yamaguchi, H., et al. 2012, PASJ, 64, 141
Uchiyama, Y., Funk, S., Katagiri, H., et al. 2012, ApJL, 749, L35
Wilms, J., Allen, A., & McCray, R. 2000, ApJ, 542, 914
Wolszczan, A., Cordes, J. M., & Dewey, R. J. 1991, ApJL, 372, L99
Yoshiike, S., Fukuda, T., Sano, H., et al. 2013, ApJ, 768, 179
Zhou, P., Safi-Harb, S., Chen, Y., et al. 2014, ApJ, 791, 87
```